https://arxiv.org/pdf/1612.03034.pdf

First test of Verlinde's theory of Emergent Gravity using Weak Gravitational Lensing measurements

Margot M. Brouwer[1]⋆, Manus R. Visser[2], Andrej Dvornik[1], Henk Hoekstra[1],
Konrad Kuijken[1], Edwin A. Valentijn[3], Maciej Bilicki[1], Chris Blake[4],
Sarah Brough[5], Hugo Buddelmeijer[1], Thomas Erben[6], Catherine Heymans[7],
Hendrik Hildebrandt[6], Benne W. Holwerda[1], Andrew M. Hopkins[5], Dominik Klaes[6],
Jochen Liske[8], Jon Loveday[9], John McFarland[3], Reiko Nakajima[6],
Cristóbal Sifón[1], Edward N. Taylor[4].

[1]*Leiden Observatory, Leiden University, Niels Bohrweg 2, 2333 CA Leiden, The Netherlands.*
[2]*Institute for Theoretical Physics, University of Amsterdam, Science Park 904, 1098 XH Amsterdam, The Netherlands.*
[3]*Kapteyn Astronomical Institute, University of Groningen, P.O. Box 800, 9700 AV Groningen, The Netherlands.*
[4]*Centre for Astrophysics and Supercomputing, Swinburne University of Technology, Hawthorn 3122, Australia.*
[5]*Australian Astronomical Observatory, P.O. Box 915, North Ryde, NSW, Australia.*
[6]*Argelander-Institut für Astronomie, Auf dem Hügel 71, D-53121 Bonn, Germany.*
[7]*SUPA, Institute for Astronomy, University of Edinburgh, Royal Observatory, Blackford Hill, Edinburgh, EH9 3HJ, UK.*
[8]*Hamburger Sternwarte, Universität Hamburg, Gojenbergsweg 112, 21029 Hamburg, Germany.*
[9]*Astronomy Centre, University of Sussex, Falmer, Brighton BN1 9QH, UK.*

ABSTRACT

Verlinde (2016) proposed that the observed excess gravity in galaxies and clusters is the consequence of Emergent Gravity (EG). In this theory the standard gravitational laws are modified on galactic and larger scales due to the displacement of dark energy by baryonic matter. EG gives an estimate of the excess gravity (described as an *apparent* dark matter density) in terms of the baryonic mass distribution and the Hubble parameter. In this work we present the first test of EG using weak gravitational lensing, within the regime of validity of the current model. Although there is no direct description of lensing and cosmology in EG yet, we can make a reasonable estimate of the expected lensing signal of low redshift galaxies by assuming a background ΛCDM cosmology. We measure the (apparent) average surface mass density profiles of 33,613 isolated central galaxies, and compare them to those predicted by EG based on the galaxies' baryonic masses. To this end we employ the ~ 180 deg^2 overlap of the Kilo-Degree Survey (KiDS) with the spectroscopic Galaxy And Mass Assembly (GAMA) survey. We find that the prediction from EG, despite requiring *no free parameters*, is in good agreement with the observed galaxy-galaxy lensing profiles in four different stellar mass bins. Although this performance is remarkable, this study is only a first step. Further advancements on both the theoretical framework and observational tests of EG are needed before it can be considered a fully developed and solidly tested theory.

Key words: gravitational lensing: weak – surveys – galaxies: haloes – cosmology: theory, dark matter – gravitation

⋆ E-mail:brouwer@strw.leidenuniv.nl

1 INTRODUCTION

In the past decades, astrophysicists have repeatedly found evidence that gravity on galactic and larger scales is in excess of the gravitational potential that can be explained by visible baryonic matter within the framework of General Relativity (GR). The first evidence through the measurements of the dynamics of galaxies in clusters (Zwicky 1937) and the Local Group (Kahn & Woltjer 1959), and through observations of galactic rotation curves (inside the optical disks by Rubin 1983, and far beyond the disks in hydrogen profiles by Bosma 1981) has been confirmed by more recent dynamical observations (Martinsson et al. 2013; Rines et al. 2013). Furthermore, entirely different methods like gravitational lensing (Hoekstra et al. 2004; Mandelbaum 2015; von der Linden et al. 2014; Hoekstra et al. 2015) of galaxies and clusters, Baryon Acoustic Oscillations (BAO's, Eisenstein et al. 2005; Blake et al. 2011) and the cosmic microwave background (CMB, Spergel et al. 2003; Planck XIII 2015) have all acknowledged the necessity of an additional mass component to explain the excess gravity. This interpretation gave rise to the idea of an invisible *dark matter* (DM) component, which now forms an important part of our standard model of cosmology. In our current ΛCDM model the additional mass density (the density parameter $\Omega_{CDM} = 0.266$ found by Planck XIII 2015) consists of cold (non-relativistic) DM particles, while the energy density in the cosmological constant ($\Omega_{\Lambda} = 0.685$) explains the observed accelerating expansion of the universe. In this paradigm, the spatial structure of the sub-dominant baryonic component (with $\Omega_b = 0.049$) broadly follows that of the DM. When a DM halo forms through the gravitational collapse of a small density perturbation (Peebles & Yu 1970) baryonic matter is pulled into the resulting potential well, where it cools to form a galaxy in the centre (White & Rees 1978). In this framework the excess mass around galaxies and clusters, which is measured through dynamics and lensing, has hitherto been interpreted as caused by this DM halo.

In this paper we test the predictions of a different hypothesis concerning the origin of the excess gravitational force: the Verlinde (2016) model of Emergent Gravity (EG). Generally, EG refers to the idea that spacetime and gravity are macroscopic notions that arise from an underlying microscopic description in which these notions have no meaning. Earlier work on the emergence of gravity has indicated that an area law for gravitational entropy is essential to derive Einstein's laws of gravity (Jacobson 1995; Padmanabhan 2010; Verlinde 2011; Faulkner et al. 2014; Jacobson 2016). But due to the presence of positive dark energy in our universe Verlinde (2016) argues that, in addition to the area law, there exists a volume law contribution to the entropy. This new volume law is thought to lead to modifications of the emergent laws of gravity at scales set by the 'Hubble acceleration scale' $a_0 = cH_0$, where c is the speed of light and H_0 the Hubble constant. In particular, Verlinde (2016) claims that the gravitational force emerging in the EG framework exceeds that of GR on galactic and larger scales, similar to the MOND phenomenology (Modified Newtonian Dynamics, Milgrom 1983) that provides a successful description of galactic rotation curves (e.g. McGaugh et al. 2016). This excess gravity can be modelled as a mass distribution of *apparent* DM, which is only determined by the baryonic mass distribution $M_b(r)$ (as a function of the spherical radius r) and the Hubble constant H_0. In a realistic cosmology, the Hubble parameter $H(z)$ is expected to evolve with redshift z. But because EG is only developed for present-day de Sitter space, any predictions on cosmological evolution are beyond the scope of the current theory. The approximation used by Verlinde (2016) is that our universe is entirely dominated by dark energy, which would imply that $H(z)$ indeed resembles a constant. In any case, a viable cosmology should at least reproduce the observed values of $H(z)$ at low redshifts, which is the regime that is studied in this work. Furthermore, at low redshifts the exact specifics of the cosmological evolution have a negligible effect on our measurements. Therefore, to calculate distances from redshifts throughout this work, we can adopt an effective ΛCDM background cosmology with $\Omega_m = 0.315$ and $\Omega_{\Lambda} = 0.685$ (Planck XIII 2015), without significantly affecting our results. To calculate the distribution of apparent DM, we use the value of $H_0 = 70\,\mathrm{km\,s^{-1}Mpc^{-1}}$. Throughout the paper we use the following definition for the reduced Hubble constant: $h \equiv h_{70} = H_0/(70\,\mathrm{km\,s^{-1}Mpc^{-1}})$.

Because, as mentioned above, EG gives an effective description of GR (with apparent DM as an additional component), we assume that a gravitational potential affects the pathway of photons as it does in the GR framework. This means that the distribution of apparent DM can be observed using the regular gravitational lensing formalism. In this work we test the predictions of EG specifically relating to galaxy-galaxy lensing (GGL): the coherent gravitational distortion of light from a field of background galaxies (sources) by the mass of a foreground galaxy sample (lenses) (see e.g. Fischer et al. 2000; Hoekstra et al. 2004; Mandelbaum et al. 2006; Velander et al. 2014; van Uitert et al. 2016). Because the prediction of the gravitational potential in EG is currently only valid for static, spherically symmetric and isolated baryonic mass distributions, we need to select our lenses to satisfy these criteria. Furthermore, as mentioned above, the lenses should be at relatively low redshifts since cosmological evolution is not yet implemented in the theory. To find a reliable sample of relatively isolated foreground galaxies at low redshift, we select our lenses from the very complete spectroscopic Galaxy And Mass Assembly survey (GAMA, Driver et al. 2011). In addition, GAMA's stellar mass measurements allow us to test the prediction of EG for four galaxy sub-samples with increasing stellar mass. The background galaxies, used to measure the lensing effect, are observed by the photometric Kilo-Degree Survey (KiDS, de Jong et al. 2013), which was specifically designed with accurate shape measurements in mind.

In Sect. 2 of this paper we explain how we select and model our lenses. In Sect. 3 we describe the lensing measurements. In Sect. 4 we introduce the EG theory and derive its prediction for the lensing signal of our galaxy sample. In Sect. 5 we present the measured GGL profiles and our comparison with the predictions from EG and ΛCDM. The discussion and conclusions are described in Sect. 6.

2 GAMA LENS GALAXIES

The prediction of the gravitational potential in EG that is tested in this work is only valid for static, spherically sym-

metric and isolated baryonic mass distributions (see Sect. 4). Ideally we would like to find a sample of isolated lenses, but since galaxies are clustered we cannot use GAMA to find galaxies that are truly isolated. Instead we use the survey to construct a sample of lenses that dominate their surroundings, and a galaxy sample that allows us to estimate the small contribution arising from their nearby low-mass galaxies (i.e. satellites). The GAMA survey (Driver et al. 2011) is a spectroscopic survey with the AAOmega spectrograph mounted on the Anglo-Australian Telescope. In this study, we use the GAMA II (Liske et al. 2015) observations over three equatorial regions (G09, G12 and G15) that together span $\sim 180 \deg^2$. Over these regions, the redshifts and properties of 180,960 galaxies[1] are measured. These data have a redshift completeness of 98.5% down to a Petrosian r-band magnitude of $m_{\rm r} = 19.8$. This is very useful to accurately determine the positional relation between galaxies, in order to find a suitable lens sample.

2.1 Isolated galaxy selection

To select foreground lens galaxies suitable for our study, we consult the 7th GAMA Galaxy Group Catalogue (G3Cv7) which is created by Robotham et al. (2011) using a Friends-of-Friends (FoF) group finding algorithm. In this catalogue, galaxies are classified as either the Brightest Central Galaxy (BCG) or a satellite of a group, depending on their luminosity and their mutual projected and line-of-sight distances. In cases where there are no other galaxies observed within the linking lengths, the galaxy remains 'non-grouped' (i.e., it is not classified as belonging to any group). Mock galaxy catalogues, which were produced using the Millennium DM simulation (Springel et al. 2005) and populated with galaxies according to the semi-analytical galaxy formation recipe 'GALFORM' (Bower et al. 2006), are used to calibrate these linking lengths and test the resulting group properties.

However, since GAMA is a flux-limited survey, it does not include the satellites of the faintest observed GAMA galaxies when these are fainter than the flux limit. Many fainter galaxies are therefore classified as non-grouped, whereas they are in reality BCGs. This selection effect is illustrated in Fig. 1, which shows that the number of non-grouped galaxies rises towards faint magnitudes whereas the number of BCGs peaks well before. The only way to obtain a sample of 'isolated' GAMA galaxies without satellites as bright as f_L times their parents luminosity, would be to select only non-grouped galaxies brighter than $1/f_L$ times the flux limit (illustrated in Fig. 1 for $f_L = 0.1$). Unfortunately such a selection leaves too small a sample for a useful lensing measurement. Moreover, we suspect that in some cases observational limitations may have prevented the detection of satellites in this sample as well. Instead, we use this selection to obtain a reasonable estimate of the satellite distribution around the galaxies in our lens sample. Because the mass of the satellites is approximately spherically distributed around the BCG, and is sub-dominant compared to the BCG's mass, we can still model the lensing signal of this component using
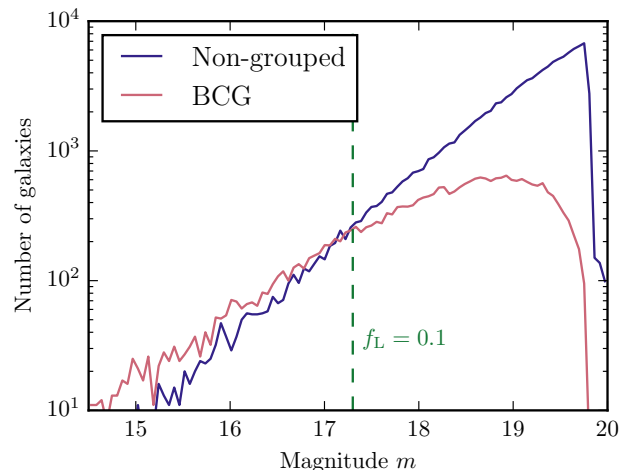
Figure 1. The magnitude distribution of non-grouped galaxies (blue) and BCGs (red). The green dashed line indicates the selection that removes galaxies which might have a satellite beyond the visible magnitude limit. These hypothetical satellites have at most a fraction $f_L = 0.1$ of the central galaxy luminosity, corresponding to the magnitude limit: $m_{\rm r} < 17.3$. We use this 'nearby' sample to obtain a reliable estimate of the satellite distribution around our centrals.

the EG theory. How we model the satellite distribution and its effect on the lensing signal is described in Sect. 2.2.3 and Sect. 4.3 respectively.

Because centrals are only classified as BCGs if their satellites are detected, whereas non-grouped galaxies are likely centrals with no observed satellites, we adopt the name 'centrals' for the combined sample of BCGs and non-grouped galaxies (i.e. all galaxies which are not satellites). As our lens sample, we select galaxies which dominate their surroundings in three ways: (i) they are centrals, i.e. not classified as satellites in the GAMA group catalogue; (ii) they have stellar masses below $10^{11} h_{70}^{-2} {\rm M}_\odot$, since we find that galaxies with higher stellar mass have significantly more satellites (see Sect. 2.2.3); and (iii) they are not affected by massive neighbouring groups, i.e. there is no central galaxy within $3 h_{70}^{-1} {\rm Mpc}$ (which is the maximum radius of our lensing measurement, see Sect. 3). This last selection suppresses the contribution of neighbouring centrals (known as the '2-halo term' in the standard DM framework) to our lensing signal, which is visible at scales above $\sim 1 h_{70}^{-1} {\rm Mpc}$.

Furthermore, we only select galaxies with redshift quality $n_{\rm Q} \geq 3$, in accordance with the standard recommendation by GAMA. After these four cuts (central, no neighbouring centrals, $M_* < 10^{11} h_{70}^{-2} {\rm M}_\odot$ and $n_{\rm Q} \geq 3$) our remaining sample of 'isolated centrals' amounts to 33, 613 lenses.

2.2 Baryonic mass distribution

Because there exists no DM component in the Verlinde (2016) framework of EG, the gravitational potential originates only from the baryonic mass distribution. Therefore, in order to determine the lensing signal of our galaxies as predicted by EG (see Sect. 4), we need to know their baryonic mass distribution. In this work we consider two possible

models: the point mass approximation and an extended mass profile. We expect the point mass approximation to be valid, given that (i) the bulk mass of a galaxy is enclosed within the minimum radius of our measurement ($R_{min} = 30\,h_{70}^{-1}\mathrm{kpc}$), and (ii) our selection criteria ensure that our isolated centrals dominate the total mass distribution within the maximum radius of our measurement ($R_{max} = 3\,h_{70}^{-1}\mathrm{Mpc}$). If these two assumptions hold, the entire mass distribution of the isolated centrals can be described by a simple point mass. This allows us to analytically calculate the lensing signal predicted by EG, based on only one observable: the galaxies' mass M_g, which consists of a stellar and a cold gas component. To asses the sensitivity of our interpretation to the mass distribution, we compare the predicted lensing signal of the point mass to that of an extended mass distribution. This more realistic extended mass profile consists of four components: stars, cold gas, hot gas and satellites, which all have an extended density profile. In the following sections we review each component, and make reasonable assumptions regarding their model profiles and corresponding input parameters.

2.2.1   Stars and cold gas

To determine the baryonic masses M_g of the GAMA galaxies, we use their stellar masses M_* from version 19 of the stellar mass catalogue, an updated version of the catalogue created by Taylor et al. (2011). These stellar masses are measured from observations of the Sloan Digital Sky Survey (SDSS, Abazajian et al. 2009) and the VISTA Kilo-Degree Infrared Galaxy survey (VIKING, Edge et al. 2013), by fitting Bruzual & Charlot (2003) stellar population synthesis models to the *ugrizZYJHK* spectral energy distributions (constrained to the rest frame wavelength range 3,000-11,000 Å). We correct M_* for flux falling outside the automatically selected aperture using the 'flux-scale' parameter, following the procedure discussed in Taylor et al. (2011).

In these models, the stellar mass includes the mass locked up in stellar remnants, but not the gas recycled back into the interstellar medium. Because the mass distribution of gas in our galaxies is not measured, we can only obtain realistic estimates from literature. There are two contributions to consider: cold gas consisting of atomic hydrogen (HI), molecular hydrogen (H_2) and helium, and hot gas consisting of ionized hydrogen and helium. Most surveys find that the mass in cold gas is highly dependent on the galaxies' stellar mass. For low-redshift galaxies ($z < 0.5$) the mass in HI (H_2) ranges from $20 - 30\%$ ($8 - 10\%$) of the stellar mass for galaxies with $M_* = 10^{10}\mathrm{M_\odot}$, dropping to $5 - 10\%$ ($4 - 5\%$) for galaxies with $M_* = 10^{11}\mathrm{M_\odot}$ (Saintonge et al. 2011; Catinella et al. 2013; Boselli et al. 2014; Morokuma-Matsui & Baba 2015). Therefore, in order to estimate the mass of the cold gas component, we consider a cold gas fraction f_{cold} which depends on the measured M_* of our galaxies. We use the best-fit scaling relation found by Boselli et al. (2014) using the Herschel Reference Survey (Boselli et al. 2010):

$$\log\left(f_{cold}\right) = \log\left(M_{cold}/M_*\right) = -0.69\log(M_*) + 6.63\,. \quad (1)$$

In this relation, the total cold gas mass M_{cold} is defined as the combination of the atomic and molecular hydrogen gas, including an additional 30% contribution of helium:

$M_{cold} = 1.3\,(M_{HI} + M_{H_2})$. With a maximum measured radius of ~ 1.5 times the effective radius of the stellar component, the extent of the cold gas distribution is very similar to that of the stars (Pohlen et al. 2010; Crocker et al. 2011; Mentuch Cooper et al. 2012; Davis et al. 2013). We therefore consider the stars and cold gas to form a single galactic mass distribution with:

$$M_g = (M_* + M_{cold}) = M_*(1 + f_{cold})\,. \quad (2)$$

For both the point mass and the extended mass profile, we use this galactic mass M_g to predict the lensing signal in the EG framework.

In the point mass approximation, the total density distribution of our galaxies consists of a point source with its mass corresponding to the galactic mass M_g of the lenses. For the extended mass profile, we use M_g as an input parameter for the density profile of the 'stars and cold gas' component. Because starlight traces the mass of this component, we use the Sérsic intensity profile (Sérsic 1963; Sersic 1968) as a reasonable approximation of the density:

$$I_S(r) \propto \rho_S(r) = \rho_e \exp\left\{-b_n\left[\left(\frac{r}{r_e}\right)^{1/n} - 1\right]\right\}\,. \quad (3)$$

Here r_e is the effective radius, n is the Sérsic index, and b_n is defined such that $\Gamma(2n) = 2\gamma(2n, b_n)$. The Sérsic parameters were measured for $167{,}600$ galaxies by Kelvin et al. (2012) on the UKIRT Infrared Deep Sky Survey Large Area Survey images from GAMA and the *ugrizYJHK* images of SDSS DR7 (where we use the parameter values as measured in the *r*-band). Of these galaxies, $69{,}781$ are contained in our GAMA galaxy catalogue. Although not all galaxies used in this work (the $33{,}613$ isolated centrals) have Sérsic parameter measurements, we can obtain a realistic estimate of the mean Sérsic parameter values of our chosen galaxy samples. We use r_e and n equal to the mean value of the galaxies for which they are measured within each sample, in order to model the density profile $\rho_S(r)$ of each full galaxy sample. This profile is multiplied by the effective mass density ρ_e, which is defined such that the mass integrated over the full $\rho_S(r)$ is equal to the mean galactic mass $\langle M_g \rangle$ of the lens sample. The mean measured values of the galactic mass and Sérsic parameters for our galaxy samples can be found in Table 1.

2.2.2   Hot gas

Hot gas has a more extended density distribution than stars and cold gas, and is generally modelled by the β-profile (e.g. Cavaliere & Fusco-Femiano 1976; Mulchaey 2000):

$$\rho_{hot}(r) = \frac{\rho_{core}}{\left(1 + (r/r_{core})^2\right)^{\frac{3\beta}{2}}}\,, \quad (4)$$

which provides a fair description of X-ray observations in clusters and groups of galaxies. In this distribution r_{core} is the core radius of the hot gas. The outer slope is characterised by β, which for a hydrostatic isothermal sphere corresponds to the ratio of the specific energy in galaxies to that in the hot gas (see e.g. Mulchaey 2000, for a review). Observations of galaxy groups indicate $\beta \sim 0.6$ (Sun et al. 2009). Fedeli et al. (2014) found similar results using the Overwhelmingly Large Simulations (OWLS, Schaye et al. 2010)

Table 1. For each stellar mass bin, this table shows the number N and mean redshift $\langle z_l \rangle$ of the galaxy sample. Next to these, it shows the corresponding measured input parameters of the ESD profiles in EG: the mean stellar mass $\langle M_* \rangle$, galactic mass $\langle M_g \rangle$, effective radius $\langle r_e \rangle$, Sérsic index $\langle n \rangle$, satellite fraction $\langle f_{sat} \rangle$ and satellite radius $\langle r_{sat} \rangle$ of the centrals. All masses are displayed in units of $\log_{10}(M/h_{70}^{-2}M_\odot)$ and all lengths in h_{70}^{-1}kpc.

$M*$-bin	N	$\langle z_l \rangle$	$\langle M_* \rangle$	$\langle M_g \rangle$	$\langle r_e \rangle$	$\langle n \rangle$	$\langle f_{sat} \rangle$	$\langle r_{sat} \rangle$
$8.5 - 10.5$	14974	0.22	10.18	10.32	3.58	1.66	0.27	140.7
$10.5 - 10.8$	10500	0.29	10.67	10.74	4.64	2.25	0.25	143.9
$10.8 - 10.9$	4076	0.32	10.85	10.91	5.11	2.61	0.29	147.3
$10.9 - 11$	4063	0.33	10.95	11.00	5.56	3.04	0.32	149.0

for the range in stellar masses that we consider here (i.e. with $M_* \sim 10^{10} - 10^{11}\,h_{70}^{-2}M_\odot$). We therefore adopt $\beta = 0.6$. Moreover, Fedeli et al. (2014) estimate that the mass in hot gas is at most 3 times that in stars. As the X-ray properties from the OWLS model of active galactic nuclei match X-ray observations well (McCarthy et al. 2010) we adopt $M_{hot} = 3\langle M_* \rangle$. Fedeli et al. (2014) find that the simulations suggest a small core radius r_{core} (i.e. even smaller than the transition radius of the stars). This implies that $\rho_{hot}(r)$ is effectively described by a single power law. Observations show a range in core radii, but typical values are tens of kpc (e.g. Mulchaey et al. 1996) for galaxy groups. We take $r_c = r_e$, which is relatively small in order to give an upper limit; a larger value would reduce the contribution of hot gas, and thus move the extended mass profile closer to the point mass case. We define the amplitude ρ_{core} of the profile such that the mass integrated over the full $\rho_{hot}(r)$ distribution is equal to the total hot gas mass M_{hot}.

2.2.3 Satellites

As described in 2.1 we use our nearby ($m_r < 17.3$) sample of centrals (BCGs and non-grouped galaxies) to find that most of the non-grouped galaxies in the GAMA catalogue might not be truly isolated, but are likely to have satellites beyond the visible magnitude limit. Fortunately, satellites are a spherically distributed, sub-dominant component of the lens, which means its (apparent) mass distribution can be described within EG. In order to assess the contribution of these satellites to our lensing signal, we first need to model their average baryonic mass distribution. We follow van Uitert et al. (2016) by modelling the density profile of satellites around the central as a double power law[2]:

$$\rho_{sat}(r) = \frac{\rho_{sat}}{(r/r_{sat})(1 + r/r_{sat})^2}\,, \qquad (5)$$

where ρ_{sat} is the density and r_{sat} the scale radius of the satellite distribution. The amplitude ρ_{sat} is chosen such that the mass integrated over the full profile is equal to the mean total mass in satellites $\langle M_*^{sat} \rangle$ measured around our nearby sample of centrals. By binning these centrals according to their stellar mass M_*^{cen} we find that, for centrals within $10^9 <$

$M_*^{cen} < 10^{11}\,h_{70}^{-2}M_\odot$, the total mass in satellites can be approximated by a fraction $f_{sat} = \langle M_*^{sat} \rangle / \langle M_*^{cen} \rangle \sim 0.2 - 0.3$. However, for centrals with masses above $10^{11}\,h_{70}^{-2}M_\odot$ the satellite mass fraction rapidly rises to $f_{sat} \sim 1$ and higher. For this reason, we choose to limit our lens sample to galaxies below $10^{11}\,h_{70}^{-2}M_\odot$. As the value of the scale radius r_{sat}, we pick the half-mass radius (the radius which contains half of the total mass) of the satellites around the nearby centrals. The mean measured mass fraction $\langle f_{sat} \rangle$ and half-mass radius $\langle r_{sat} \rangle$ of satellites around centrals in our four M_*-bins can be found in Table 1.

3 LENSING MEASUREMENT

According to GR, the gravitational potential of a mass distribution leaves an imprint on the path of travelling photons. As discussed in Sect. 1, EG gives an effective description of GR (where the excess gravity from apparent DM detailed in Verlinde 2016 is an additional component). We therefore work under the assumption that a gravitational potential (including that of the predicted apparent DM distribution) has the exact same effect on light rays as in GR. Thus, by measuring the coherent distortion of the images of faraway galaxies (sources), we can reconstruct the projected (apparent) mass distribution (lens) between the background sources and the observer. In the case of GGL, a large sample of foreground galaxies acts as the gravitational lens (for a general introduction, see e.g. Bartelmann & Schneider 2001; Schneider et al. 2006). Because the distortion of the source images is only $\sim 1\%$ of their intrinsic shape, the tangential shear γ_t (which is the source ellipticity tangential to the line connecting the source and the centre of the lens) is averaged for many sources within circular annuli around the lens centre. This measurement provides us with the average shear $\langle \gamma_t \rangle(R)$ as a function of projected radial distance R from the lens centres. In GR, this quantity is related to the Excess Surface Density (ESD) profile $\Delta\Sigma(R)$. Using our earlier assumption, we can also use the same methodology to obtain the ESD of the apparent DM in the EG framework. The ESD is defined as the average surface mass density $\langle \Sigma \rangle(< R)$ within R, minus the surface density $\Sigma(R)$ at that radius:

$$\Delta\Sigma(R) = \langle \Sigma \rangle(< R) - \Sigma(R) = \langle \gamma_t \rangle(R)\,\Sigma_{crit}\,. \qquad (6)$$

Here Σ_{crit} is the critical surface mass density at the redshift of the lens:

$$\Sigma_{crit} = \frac{c^2}{4\pi G}\frac{D(z_s)}{D(z_l)\,D(z_l, z_s)}\,, \qquad (7)$$

---

[2] Although this double power law is mathematically equivalent to the Navarro-Frenk-White profile (Navarro et al. 1995) which describes virialized DM halos, it is in our case not related to any (apparent) DM distribution. It is merely an empirical fit to the measured distribution of satellite galaxies around their central galaxy.

a geometrical factor that is inversely proportional to the strength of the lensing effect. In this equation $D(z_l)$ and $D(z_s)$ are the angular diameter distances to the lens and source respectively, and $D(z_l, z_s)$ is the distance between the lens and the source.

For a more extensive discussion of the GGL method and the role of the KiDS and GAMA surveys therein, we refer the reader to previous KiDS-GAMA lensing papers: Sifón et al. (2015); van Uitert et al. (2016); Brouwer et al. (2016) and especially Sect. 3 of Viola et al. (2015).

3.1 KiDS source galaxies

The background sources used in our GGL measurements are observed by KiDS (de Jong et al. 2013). The KiDS photometric survey uses the OmegaCAM instrument (Kuijken et al. 2011) on the VLT Survey Telescope (Capaccioli & Schipani 2011) which was designed to provide a round and uniform point spread function (PSF) over a square degree field of view, specifically with weak lensing measurements in mind. Of the currently available $454\,\mathrm{deg}^2$ area from the 'KiDS-450' data release (Hildebrandt et al. 2016) we use the $\sim 180\,\mathrm{deg}^2$ area that overlaps with the equatorial GAMA fields (Driver et al. 2011). After masking bright stars and image defects, 79% of our original survey overlap remains (de Jong et al. 2015).

The photometric redshifts of the background sources are determined from *ugri* photometry as described in Kuijken et al. (2015) and Hildebrandt et al. (2016). Due to the bias inherent in measuring the source redshift probability distribution $p(z_s)$ of each individual source (as was done in the previous KiDS-GAMA studies), we instead employ the source redshift number distribution $n(z_s)$ of the full population of sources. The individual $p(z_s)$ is still measured, but only to find the 'best' redshift z_B at the $p(z_s)$-peak of each source. Following Hildebrandt et al. (2016) we limit the source sample to: $z_B < 0.9$. We also use z_B in order to select sources which lie sufficiently far behind the lens: $z_B > z_l + 0.2$. The $n(z_s)$ is estimated from a spectroscopic redshift sample, which is re-weighted to resemble the photometric properties of the appropriate KiDS galaxies for different lens redshifts (for details, see Sect. 3 of Hildebrandt et al. 2016 and van Uitert et al. 2016). We use the $n(z)$ distribution behind the lens for the calculation of the critical surface density from Eq. (7):

$$\Sigma_{\mathrm{crit}}^{-1} = \frac{4\pi G}{c^2} D(z_l) \int_{z_l + 0.2}^{\infty} \frac{D(z_l, z_s)}{D(z_s)} n(z_l, z_s)\,\mathrm{d}z_s \,, \qquad (8)$$

By assuming that the intrinsic ellipticities of the sources are randomly oriented, $\langle \gamma_t \rangle$ from Eq. (6) can be approximated by the average tangential ellipticity $\langle \epsilon_t \rangle$ given by:

$$\epsilon_t = -\epsilon_1 \cos(2\phi) - \epsilon_2 \sin(2\phi) \,, \qquad (9)$$

where ϵ_1 and ϵ_2 are the measured source ellipticity components, and ϕ is the angle of the source relative to the lens centre (both with respect to the equatorial coordinate system). The measurement of the source ellipticities is performed on the r-band data, which is observed under superior observing conditions compared to the other bands (de Jong et al. 2015; Kuijken et al. 2015). The images are reduced by the THELI pipeline (Erben et al. 2013 as described in Hildebrandt et al.

2016). The sources are detected from the reduced images using the SEXTRACTOR algorithm (Bertin & Arnouts 1996), whereafter the ellipticities of the source galaxies are measured using the improved self-calibrating *lens*fit code (Miller et al. 2007, 2013; Fenech Conti et al. 2016). Each shape is assigned a weight w_s that reflects the reliability of the ellipticity measurement. We incorporate this *lens*fit weight and the lensing efficiency $\Sigma_{\mathrm{crit}}^{-1}$ into the total weight:

$$W_{ls} = w_s \Sigma_{\mathrm{crit}}^{-2} \,, \qquad (10)$$

which is applied to each lens-source pair. This factor downweights the contribution of sources that have less reliable shape measurements, and of lenses with a redshift closer to that of the sources (which makes them less sensitive to the lensing effect).

Inside each radial bin R, the weights and tangential ellipticities of all lens-source pairs are combined according to Eq. (6) to arrive at the ESD profile:

$$\Delta\Sigma(R) = \frac{1}{1+K} \frac{\sum_{ls} W_{ls} \epsilon_t \Sigma_{\mathrm{crit},l}}{\sum_{ls} W_{ls}} \,. \qquad (11)$$

In this equation, K is the average correction of the multiplicative bias m on the *lens*fit shear estimates. The values of m are determined using image simulations (Fenech Conti et al. 2016) for 8 tomographic redshift slices between $0.1 \leq z_B < 0.9$ (Dvornik et al., in prep). The average correction is computed for the lens-source pairs in each respective redshift slice as follows:

$$K = \frac{\sum_{ls} W_{ls} m_s}{\sum_{ls} W_{ls}} \,, \qquad (12)$$

where the mean value of K over the entire source redshift range is -0.014.

We also correct the ESD for systematic effects that arise from the residual shape correlations due to PSF anisotropy. This results in non-vanishing contributions to the ESD signal on large scales and at the survey edges, because the averaging is not done over all azimuthal angles. This spurious signal can be determined by measuring the lensing signal around random points. We use ~ 18 million locations from the GAMA random catalogue, and find that the resulting signal is small (below 10% for scales up to $\sim 1\,h_{70}^{-1}\,\mathrm{Mpc}$). We subtract the lensing signal around random locations from all measured ESD profiles.

Following previous KiDS-GAMA lensing papers, we measure the ESD profile for 10 logarithmically spaced radial bins within $0.02 < R < 2\,h_{100}^{-1}\mathrm{Mpc}$, where our estimates of the signal and uncertainty are thoroughly tested[3]. However, since we work with the $h \equiv h_{70}$ definition, we use the approximately equivalent $0.03 < R < 3\,h_{70}^{-1}\mathrm{Mpc}$ as our radial distance range. The errors on the ESD values are given by the diagonal of the analytical covariance matrix. Section 3.4 of Viola et al. (2015) includes the computation of the analytical covariance matrix and shows that, up to a projected radius of $R = 2\,h_{100}^{-1}\mathrm{Mpc}$, the square root of the diagonal is in agreement with the error estimate from bootstrapping.

---

[3] Viola et al. (2015) used the following definition of the reduced Hubble constant: $h \equiv h_{100} = H_0/(100\,\mathrm{km\,s}^{-1}\mathrm{Mpc}^{-1})$

4 LENSING SIGNAL PREDICTION

According to Verlinde (2016), the gravitational potential $\Phi(r)$ caused by the enclosed baryonic mass distribution $M_b(r)$ exceeds that of GR on galactic and larger scales. In addition to the normal GR contribution of $M_b(r)$ to $\Phi(r)$, there exists an extra gravitational effect. This excess gravity arises due to a volume law contribution to the entropy that is associated with the positive dark energy in our universe. In a universe without matter the total entropy of the dark energy would be maximal, as it would be non-locally distributed over all available space. In our universe, on the other hand, any baryonic mass distribution $M_b(r)$ reduces the entropy content of the universe. This removal of entropy due to matter produces an elastic response of the underlying microscopic system, which can be observed on galactic and larger scales as an additional gravitational force. Although this excess gravity does not originate from an actual DM contribution, it can be effectively described by an *apparent* DM distribution $M_D(r)$.

4.1 The apparent dark matter formula

Verlinde (2016) determines the amount of apparent DM by estimating the elastic energy associated with the entropy displacement caused by $M_b(r)$. This leads to the following relation[4]:

$$\int_0^r \varepsilon_D^2(r') A(r') dr' = V_{M_b}(r), \tag{13}$$

where we integrate over a sphere with radius r and area $A(r) = 4\pi r^2$. The strain $\varepsilon_D(r)$ caused by the entropy displacement is given by:

$$\varepsilon_D(r) = \frac{8\pi G}{cH_0} \frac{M_D(r)}{A(r)}, \tag{14}$$

where c is the speed of light, G the gravitational constant, and H_0 the present-day Hubble constant (which we choose to be $H_0 = 70\,\mathrm{km\,s^{-1}Mpc^{-1}}$). Furthermore, $V_{M_b}(r)$ is the volume that would contain the amount of entropy that is removed by a mass M_b inside a sphere of radius r, if that volume were filled with the average entropy density of the universe:

$$V_{M_b}(r) = \frac{8\pi G}{cH_0} \frac{M_b(r)\, r}{3}. \tag{15}$$

Now inserting the relations (14) and (15) into (13) yields:

$$\int_0^r \frac{G M_D^2(r')}{r'^2} dr' = M_b(r) r \frac{cH_0}{6}. \tag{16}$$

Finally, by taking the derivative with respect to r on both sides of the equation, one arrives at the following relation:

$$M_D^2(r) = \frac{cH_0 r^2}{6G} \frac{d\,(M_b(r)r)}{dr}. \tag{17}$$

This is the apparent DM formula from Verlinde (2016), which translates a baryonic mass distribution into an apparent DM distribution. This apparent DM only plays a role in the regime where the elastic response of the entropy

of dark energy S_{DE} takes place: where $V(r) > V_{M_b}(r)$, i.e. $S_{DE} \propto V(r)$ is large compared to the entropy that is removed by $M_b(r)$ within our radius r. By substituting Eq. (15) into this condition, we find that this is the case when:

$$r > \sqrt{\frac{2G}{cH_0} M_b(r)}. \tag{18}$$

For a lower limit on this radius for our sample, we can consider a point source with a mass of $M = 10^{10}\,h_{70}^{-2}\mathrm{M_\odot}$, close to the average mass $\langle M_g \rangle$ of galaxies in our lowest stellar mass bin. In this simple case, the regime starts when $r > 2\,h_{70}^{-1}\mathrm{kpc}$. This shows that our observations (which start at $30\,h_{70}^{-1}\mathrm{kpc}$) are well within the EG regime.

However, it is important to keep in mind that this equation does not represent a new fundamental law of gravity, but is merely a macroscopic approximation used to describe an underlying microscopic phenomenon. Therefore, this equation is only valid under the specific set of circumstances that have been assumed for its derivation. In this case, the system considered was a static, spherically symmetric and isolated baryonic mass distribution. With these limitations in mind, we have selected our galaxy sample to meet these criteria as closely as possible (see Sect. 2.1).

Finally we note that, in order to test the EG predictions with gravitational lensing, we need to make some assumptions about the used cosmology (as discussed in Sect. 1). These concern the geometric factors in the lensing equation (Eq. 7), and the evolution of the Hubble constant (which enters in Eq. (17) for the apparent DM). We assume that, if EG is to be a viable theory, it should predict an expansion history that agrees with the current supernova data (Riess et al. 1996; Kessler et al. 2009; Betoule et al. 2014), specifically over the redshift range that is relevant for our lensing measurements ($0.2 < z_s < 0.9$). If this is the case, the angular diameter distance-redshift relation is similar to what is used in ΛCDM. We therefore adopt a ΛCDM background cosmology with $\Omega_m = 0.315$ and $\Omega_\Lambda = 0.685$, based on the Planck XIII (2015) measurements. Regarding H_0 in Eq. (17), we note that a Hubble parameter that changes with redshift is not yet implemented in the EG theory. However, for the lens redshifts considered in this work ($\langle z_l \rangle \sim 0.2$) the difference resulting from using H_0 or $H(z_l)$ to compute the lensing signal prediction is $\sim 5\%$. This means that, considering the statistical uncertainties in our measurements ($\gtrsim 40\%$, see e.g. Fig. 2), our choice to use $H_0 = 70\,\mathrm{km\,s^{-1}Mpc^{-1}}$ instead of an evolving $H(z_l)$ has no significant effect on the results of this work.

From Eq. (17) we now need to determine the ESD profile of the apparent DM distribution, in order to compare the predictions from EG to our measured GGL profiles. The next steps toward this $\Delta\Sigma_{EG}(R)$ depend on our assumptions regarding the baryonic mass distribution of our lenses. We compute the lensing signal in EG for two models (which are discussed in Sect. 2.2): the point mass approximation and the more realistic extended mass distribution.

4.2 Point mass approximation

In this work we measure the ESD profiles of galaxies at projected radial distances $R > 30\,h_{70}^{-1}\mathrm{kpc}$. If we assume that, beyond this distance, the galaxy is almost entirely enclosed

---

[4] Although Verlinde (2016) derives his relations for an arbitrary number of dimensions d, for the derivation in this paper we restrict ourselves to four spacetime dimensions.

within the radius r, we can approximate the enclosed baryonic mass as a constant: $M_{\rm b}(r) = M_{\rm b}$. Re-writing Eq. (17) accordingly yields:

$$M_{\rm D}(r) = \sqrt{\frac{cH_0}{6\,G}}\, r\sqrt{M_{\rm b}} \equiv C_{\rm D}\, r\sqrt{M_{\rm b}}\,, \qquad (19)$$

where $C_{\rm D}$ is a constant factor determined by c, G and H_0. In order to calculate the resulting $\Delta\Sigma_{\rm D}(R)$ we first need to determine the spherical density distribution $\rho_{\rm D}(r)$. Under the assumption of spherical symmetry, we can use:

$$\rho_{\rm D}(r) = \frac{1}{4\pi r^2}\frac{dM_{\rm D}(r)}{dr} = \frac{C_{\rm D}\sqrt{M_{\rm b}}}{4\pi r^2}\,. \qquad (20)$$

We calculate the corresponding surface density $\Sigma_{\rm D}(R)$ as a function of projected distance R in the cylindrical coordinate system (R, ϕ, z), where z is the distance along the line-of-sight and $r^2 = R^2 + z^2$, such that:

$$\Sigma_{\rm D}(R) = \int_{-\infty}^{\infty} \rho_{\rm D}(R, z)\,{\rm d}z\,. \qquad (21)$$

Substituting $\rho_{\rm D}(R, z)$ provides the surface density of the apparent DM distribution associated with our point mass:

$$\Sigma_{\rm D}(R) = \frac{C_{\rm D}\sqrt{M_{\rm b}}}{4\pi}\, 2\int_0^{\infty}\frac{{\rm d}z}{R^2 + z^2} = \frac{C_{\rm D}\sqrt{M_{\rm b}}}{4R}\,. \qquad (22)$$

We can now use Eq. (6) to find the ESD:

$$\Delta\Sigma(R) = \langle\Sigma\rangle(< R) - \Sigma(R) =$$
$$\frac{2\pi\int_0^R \Sigma(R')R'\,{\rm d}R'}{\pi R^2} - \Sigma(R)\,. \qquad (23)$$

In the case of our point mass:

$$\Delta\Sigma_{\rm D}(R) = \frac{C_{\rm D}\sqrt{M_{\rm b}}}{2R} - \frac{C_{\rm D}\sqrt{M_{\rm b}}}{4R} = \frac{C_{\rm D}\sqrt{M_{\rm b}}}{4R}\,, \qquad (24)$$

which happens to be equal to $\Sigma_{\rm D}(R)$ from Eq. (22)[5].

Apart from the extra contribution from the apparent DM predicted by EG, we also need to add the standard GR contribution from baryonic matter to the ESD. Under the assumption that the galaxy is a point mass we know that $\Sigma_{\rm b}(R) = 0$ for $R > 0$, and that the integral over $\Sigma_{\rm b}(R)$ must give the total mass $M_{\rm b}$ of the galaxy. Substituting this into Eq. (23) gives us:

$$\Delta\Sigma_{\rm b}(R) = \frac{M_{\rm b}}{\pi R^2}\,. \qquad (25)$$

Ultimately, the total ESD predicted by EG in the point mass approximation is:

$$\Delta\Sigma_{\rm EG}(R) = \Delta\Sigma_{\rm b}(R) + \Delta\Sigma_{\rm D}(R)\,, \qquad (26)$$

where the contributions are the ESDs of a point source with mass $M_{\rm g}$ of our galaxies, both in GR and EG.

---

[5] Note that the ESD of the apparent DM distribution: $\Delta\Sigma_{\rm D}(R) \propto \sqrt{H_0 M_{\rm b}}/R \propto \sqrt{h}$, is explicitly dependent on the Hubble constant, which means that an incorrect measured value of H_0 would affect our conclusions.

4.3 Extended mass distribution

The above derivation only holds under the assumption that our galaxies can be considered point masses. To test whether this is justified, we wish to compare the point mass prediction to a more realistic lens model. This model includes the extended density profile for stars, cold gas, hot gas and satellites as described in Sect. 2.2. To determine the ESD profile of the extended galaxy model as predicted by EG, we cannot perform an analytical calculation as we did for the point mass approximation. Instead we need to calculate the apparent DM distribution $M_{\rm D}^{\rm ext}(r)$ and the resulting $\Delta\Sigma_{\rm D}^{\rm ext}(R)$ numerically for the sum of all baryonic components. We start out with the total spherical density distribution $\rho_{\rm b}^{\rm ext}(r)$ of all components:

$$\rho_{\rm b}^{\rm ext}(r) = \rho_{\rm b}^{\rm S}(r) + \rho_{\rm b}^{\rm hot}(r) + \rho_{\rm b}^{\rm sat}(r)\,, \qquad (27)$$

where the respective contributions are: the Sérsic model for stars and cold gas, the β-profile for hot gas, and the double power law for satellites. We numerically convert this to the enclosed mass distribution:

$$M_{\rm b}^{\rm ext}(r) = 4\pi\int_0^r \rho_{\rm b}^{\rm ext}(r')r'^2\,{\rm d}r'\,. \qquad (28)$$

We rewrite Eq. (17) in order to translate $M_{\rm b}^{\rm ext}(r)$ to its corresponding distribution of apparent DM in EG:

$$M_{\rm D}^{\rm ext}(r) = C_{\rm D}r\sqrt{\frac{dM_{\rm b}^{\rm ext}(r)\,r}{dr}}\,, \qquad (29)$$

which is numerically converted into the apparent DM density distribution $\rho_{\rm D}^{\rm ext}(r)$ by substituting $M_{\rm D}^{\rm ext}(r)$ into Eq. (20).

The projected surface density $\Sigma_{\rm D}^{\rm ext}(R)$ from Eq. (21) is calculated by computing the value of $\rho_{\rm D}^{\rm ext}(R, z)$ in cylindrical coordinates for 10^3 values of z and integrating over them. The last step towards computing the ESD profile is the subtraction of $\Sigma_{\rm D}^{\rm ext}(R)$ from the average surface density within R, as in Eq. (23), where $\langle\Sigma_{\rm D}^{\rm ext}\rangle(< R)$ is calculated by performing the cumulative sum over $2\pi R\,\Sigma_{\rm D}^{\rm ext}(R)$ and dividing the result by its cumulative area. In addition to the lensing signal from apparent DM, we need to include the baryonic ESD profile. We numerically compute $\Delta\Sigma_{\rm b}^{\rm ext}(R)$ from $\rho_{\rm b}^{\rm ext}(r)$ in the same way as we computed $\Delta\Sigma_{\rm D}^{\rm ext}(R)$ from $\rho_{\rm D}^{\rm ext}(r)$. This makes the total ESD predicted by EG for the extended mass distribution:

$$\Delta\Sigma_{\rm EG}^{\rm ext}(R) = \Delta\Sigma_{\rm b}^{\rm ext}(R) + \Delta\Sigma_{\rm D}^{\rm ext}(R)\,. \qquad (30)$$

When considering the resulting ESD profiles of the extended density models, we must keep in mind that they only represent reasonable estimates which contain uncertainties for two different reasons:

(i) The extended baryonic density distribution of each component is approximated using reasonable assumptions on the used model profiles and their corresponding input parameters. These assumptions are based on observations of the galaxies in our sample and of other galaxies, and also on simulations. Although we try to find suitable input parameters corresponding to the measured stellar mass of our galaxy samples, we cannot be certain that our modelled density distributions are completely correct.

(ii) We cannot model the extended density distribution for each individual GAMA galaxy, but have to assume one average profile per lens sample (based on the average stellar mass $\langle M_* \rangle$ of that sample). Translating the extended baryonic mass model to the lensing profile of its corresponding apparent DM distribution (as explained above) is a highly non-linear operation. Therefore, we cannot be certain that the calculated lensing profile of an average density distribution is exactly the same as the lensing profile of all individual galaxies combined, although these would only differ greatly in the unlikely case that there is a large spread in the input parameters of the extended mass profiles within each stellar mass sub-sample.

For these two reasons we cannot use the average profile as a reliable model for the apparent DM lensing signal of our galaxy samples. In the point mass approximation, we do have the measured input parameter (the stellar mass) for each individual galaxy, and we can compute the apparent DM lensing profile for each individual galaxy. However, this approach can only be used when the contribution from hot gas and satellites is small. We therefore compare our estimate of the apparent DM lensing profile of the extended mass distribution to that of the point masses, to assess the error margins in our EG prediction.

The total ESD profile predicted for the extended density distribution, and that of each component[6], is shown in Fig. 2. We only show the profiles for the galaxies in our highest stellar mass bin: $10^{10.9} < M_* < 10^{11} \, h_{70}^{-2} \mathrm{M}_\odot$, but since the relations between the mass in hot gas, satellites and their galaxies are approximately linear, the profiles look similar for the other sub-samples. At larger scales, we find that the point mass approximation predicts a lower ESD than the extended mass profile. However, the difference between the $\Delta\Sigma(R)$ predictions of these two models is comparable to the median 1σ uncertainty on the ESD of our sample (which is illustrated by the gray band in Fig. 2). We conclude that, given the current statistical uncertainties in the lensing measurements, the point mass approximation is adequate for isolated centrals within the used radial distance range ($0.03 < R < 3 \, h_{70}^{-1} \mathrm{Mpc}$).

5 RESULTS

We measure the ESD profiles (following Sect. 3) of our sample of isolated centrals, divided into four sub-samples of increasing stellar mass. The boundaries of the M_*-bins: $\log(M_*/ h_{70}^{-2}\mathrm{M}_\odot) = [8.5, 10.5, 10.8, 10.9, 11.0]$, are chosen to maintain an approximately equal signal-to-noise in each bin. Figure 3 shows the measured ESD profiles (with 1σ error bars) of galaxies in the four M_*-bins. Together with these measurements we show the ESD profile predicted by EG, under the assumption that our isolated centrals can be considered point masses at scales within $0.03 < R < 3 \, h_{70}^{-1} \mathrm{Mpc}$. The masses M_g of the galaxies in each bin serve as input in Eq. (26), which provides the ESD profiles predicted by

---

[6] Note that, due to the non-linear nature of the calculation of the apparent DM distribution, the total ESD profile of the extended mass distribution is not the sum of the components shown in Fig. 2.

Table 2. For each stellar mass bin, this table shows the median values (including 16th and 84th percentile error margins) of the halo mass M_h obtained by the NFW fit, and the 'best' amplitude A_B that minimizes the χ^2 if the EG profile were multiplied by it (for the point mass and extended mass profile). The halo masses are displayed in units of $\log_{10}(M/ h_{70}^{-2}\mathrm{M}_\odot)$.

M_*-bin	M_h	A_B	$A_\mathrm{B}^{\mathrm{ext}}$
$8.5 - 10.5$	$12.15^{+0.10}_{-0.11}$	$1.36^{+0.21}_{-0.21}$	$1.21^{+0.19}_{-0.19}$
$10.5 - 10.8$	$12.45^{+0.10}_{-0.11}$	$1.32^{+0.19}_{-0.19}$	$1.20^{+0.18}_{-0.18}$
$10.8 - 10.9$	$12.43^{+0.17}_{-0.22}$	$1.07^{+0.27}_{-0.27}$	$0.94^{+0.25}_{-0.25}$
$10.9 - 11$	$12.62^{+0.13}_{-0.16}$	$1.33^{+0.25}_{-0.26}$	$1.20^{+0.23}_{-0.24}$

EG for each individual galaxy. The mean baryonic masses of the galaxies in each M_*-bin can be found in Table 1. The ESDs of the galaxies in each sample are averaged to obtain the total $\Delta\Sigma_{\mathrm{EG}}(R)$. It is important to note that the shown EG profiles do *not contain any free parameters*: both their slope and amplitudes are fixed by the prediction from the EG theory (as stated in Eq. 17) and the measured masses M_g of the galaxies in each M_*-bin. Although this is only a first attempt at testing the EG theory using lensing data, we can perform a very simple comparison of this prediction with both the lensing observations and the prediction from the standard ΛCDM model.

5.1 Model comparison

In standard GGL studies performed within the ΛCDM framework, the measured ESD profile is modelled by two components: the baryonic mass of the galaxy and its surrounding DM halo. The baryonic component is often modelled as a point source with the mean baryonic mass of the galaxy sample, whereas the DM halo component usually contains several free parameters, such as the mass and concentration of the halo, which are evaluated by fitting a model to the observed ESD profiles. Motivated by N-body simulations, the DM halo is most frequently modelled by the Navarro-Frenk-White density profile (NFW, Navarro et al. 1995), very similar to the double power law in Eq. (5). This profile has two free parameters: the halo mass M_h, which gives the amplitude, and the scale radius r_s, which determines where the slope changes. Following previous GAMA-KiDS lensing papers (see e.g. Sifón et al. 2015; Viola et al. 2015; van Uitert et al. 2016; Brouwer et al. 2016) we define M_h as M_{200}: the virial mass contained within r_{200}, and we define the scale radius in terms of the concentration: $c \equiv r_{200}/r_\mathrm{s}$. In these definitions, r_{200} is the radius that encloses a density of 200 times $\rho_\mathrm{m}(z)$, the average matter density of the universe. Using the Duffy et al. (2008) mass-concentration relation, we can define c in terms of M_h. We translate the resulting density profile, which depends exclusively on the DM halo mass, into the projected ESD distribution following the analytical description of Wright & Brainerd (2000). We combine this NFW model with a point mass that models the baryonic galaxy component (as in Eq. 25). Because our lens selection minimizes the contribution from neighbouring centrals (see Sect. 2.1), we do not need to add a component that fits the 2-halo term. We fit the NFW model to our measured ESD profiles using the EMCEE
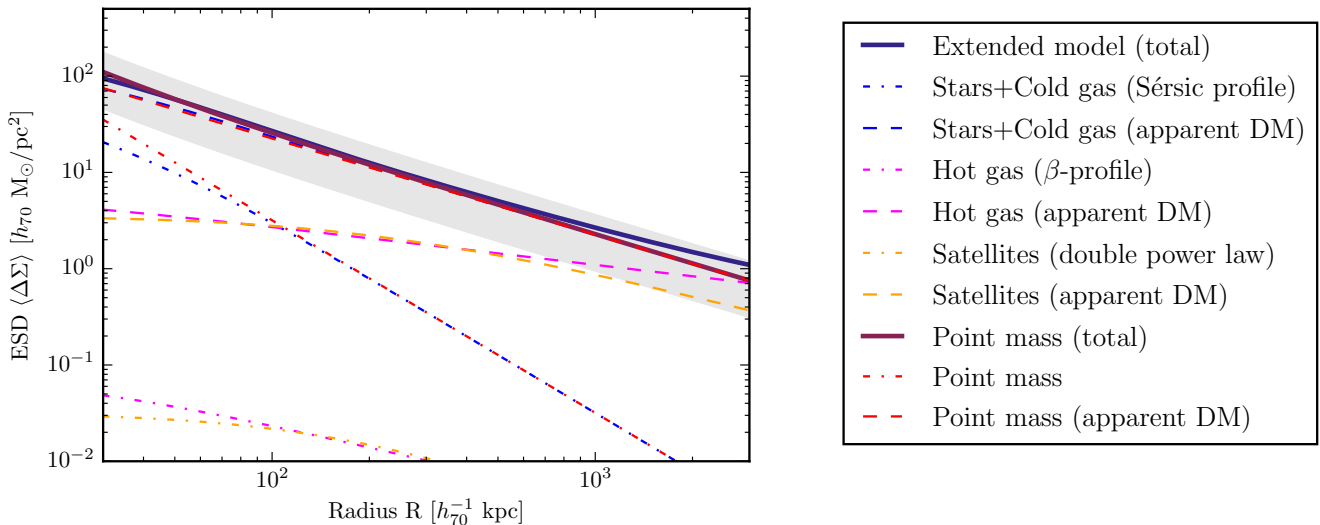
Figure 2. The ESD profile predicted by EG for isolated centrals, both in the case of the point mass approximation (dark red, solid) and the extended galaxy model (dark blue, solid). The former consists of a point source with the mass of the stars and cold gas component (red), with the lensing signal evaluated for both the baryonic mass (dash-dotted) and the apparent DM (dashed). The latter consists of a stars and cold gas component modelled by a Sérsic profile (blue), a hot gas component modelled by a β-profile (magenta), and a satellite distribution modelled by a double power law (orange), all with the lensing signal evaluated for both the baryonic mass (dash-dotted) and the apparent DM (dashed). Note that the total ESD of the extended mass distribution is not equal to the sum of its components, due to the non-linear conversion from baryonic mass to apparent DM. All profiles are shown for our highest mass bin ($10^{10.9} < M_* < 10^{11} \, h_{70}^{-2} \mathrm{M_\odot}$), but the difference between the two models is similar for the other galaxy sub-samples. The difference between the ESD predictions of the two models is comparable to the median 1σ uncertainty on our lensing measurements (illustrated by the grey band).

sampler (Foreman-Mackey et al. 2013) with 100 walkers performing 1000 steps. The model returns the median posterior values of M_h (including 16th and 84th percentile error margins) displayed in Table 2. The best-fit ESD profile of the NFW model (including 16th and 84th percentile bands) is shown in Fig. 3.

For both the $\Delta\Sigma_\mathrm{EG}$ predicted by EG (in the point mass approximation) and the simple NFW fit $\Delta\Sigma_\mathrm{NFW}$, we can compare the $\Delta\Sigma_\mathrm{mod}$ of the model with the observed $\Delta\Sigma_\mathrm{obs}$ by calculating the χ^2 value:

$$\chi^2 = (\Delta\Sigma_\mathrm{obs} - \Delta\Sigma_\mathrm{mod})^\intercal \cdot C^{-1} (\Delta\Sigma_\mathrm{obs} - \Delta\Sigma_\mathrm{mod}), \quad (31)$$

where C^{-1} is the inverse of the analytical covariance matrix (see Sect. 3). From this quantity we can calculate the reduced χ^2 statistic[7]: $\chi^2_\mathrm{red} = \chi^2/N_\mathrm{DOF}$. It depends on the number of degrees of freedom (DOF) of the model: $N_\mathrm{DOF} = N_\mathrm{data} - N_\mathrm{param}$, where N_data is the number of datapoints in the measurement and N_param is the number of free parameters. Due to our choice of 10 R-bins and 4 M_*-bins, we use $4 \times 10 = 40$ data-points. In the case of EG there are no free parameters, which means $N_\mathrm{DOF}^\mathrm{EG} = 40$. Our simple NFW model has one free parameter M_h for each M_*-bin, resulting in $N_\mathrm{DOF}^\mathrm{NFW} = 40 - 4 = 36$. The resulting total χ^2_red over the four M_*-bins is $44.82/40 = 1.121$ for EG, and $33.58/36 = 0.933$ for the NFW fit. In other words, both the NFW and EG prediction agree quite well with the measured

ESD profile, where the NFW fit has a slightly better χ^2_red value. Since the NFW profile is an empirical description of the surface density of virialized systems, the apparent correspondence of both the NFW fit and the EG prediction with the observed ESD essentially reflects that the predicted EG profile roughly follows that of virialized systems.

A more appropriate way to compare the two models, however, is in the Bayesian framework. We use a very simple Bayesian approach by computing the Bayesian Information Criterion (BIC, Schwarz 1978). This criterion, which is based on the maximum likelihood $\mathcal{L}_\mathrm{max}$ of the data given a model, penalizes model complexity more strongly than the χ^2_red. This model comparison method is closely related to other information criteria such as the Akaike Information Criterion (AIK, Akaike 1973) which have become popular because they only require the likelihood at its maximum value, rather than in the whole parameter space, to perform a model comparison (see e.g. Liddle 2007). This approximation only holds when the posterior distribution is Gaussian and the data points are independent. Calculating the BIC, which is defined as:

$$BIC = -2\ln(\mathcal{L}_\mathrm{max}) + N_\mathrm{param} \ln(N_\mathrm{data}), \quad (32)$$

allows us to consider the relative evidence of two competing models, where the one with the lowest BIC is preferred. The difference ΔBIC gives the significance of evidence against the higher BIC, ranging from "0 - 2: Not worth more than a bare mention" to ">10: Very strong" (Kass & Raftery 1995). In the Gaussian case, the likelihood can be rewritten as: $-2\ln(\mathcal{L}_\mathrm{max}) = \chi^2$. Using this method, we find that $BIC_\mathrm{EG} = 44.82$ and $BIC_\mathrm{NFW} = 48.33$. This shows that,

---

[7] While the reduced χ^2 statistic is shown to be a suboptimal goodness-of-fit estimator (see e.g. Andrae et al. 2010) it is a widely used criterion, and we therefore discuss it here for completeness.
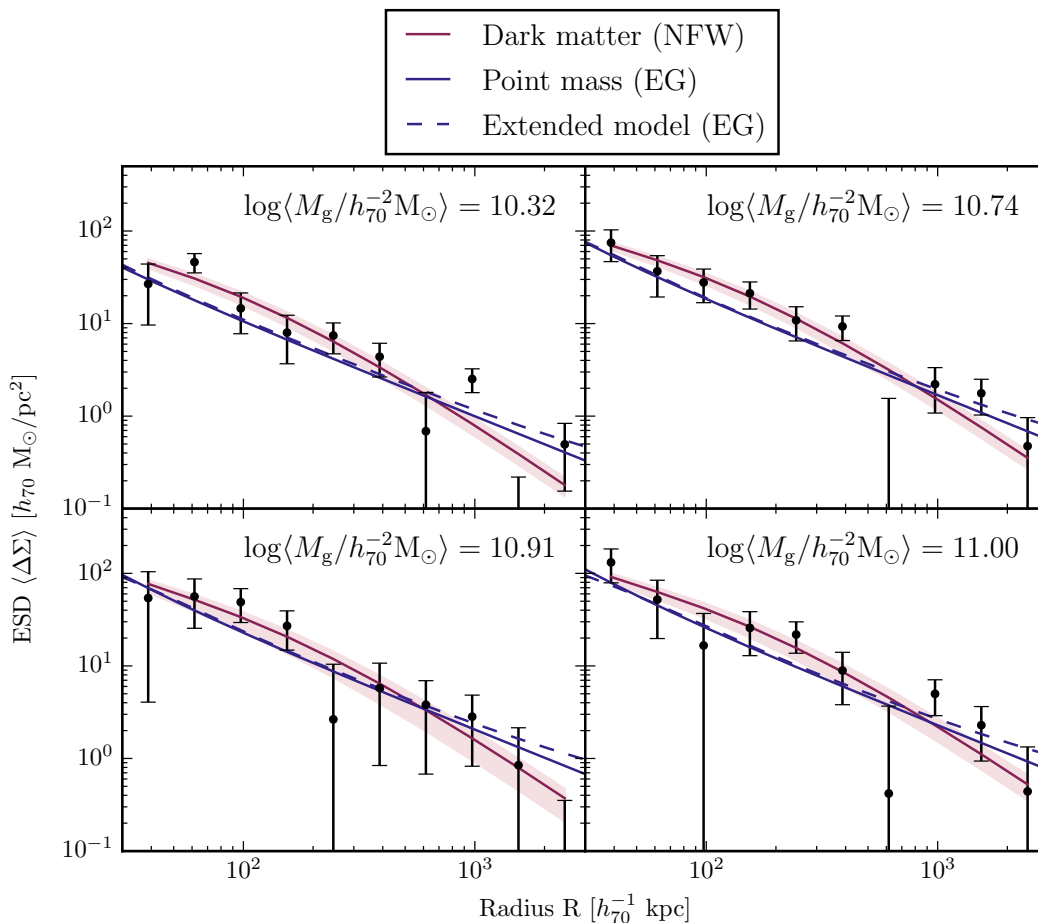
Figure 3. The measured ESD profiles of isolated centrals with 1σ error bars (black), compared to those predicted by EG in the point mass approximation (blue) and for the extended mass profile (blue, dashed). Note that *none of these predictions are fitted to the data*: they follow directly from the EG theory by substitution of the baryonic masses M_{g} of the galaxies in each sample (and, in the case of the extended mass profile, reasonable assumptions for the other baryonic mass distributions). The mean measured galaxy mass is indicated at the top of each panel. For comparison we show the ESD profile of a simple NFW profile as predicted by GR (red), with the DM halo mass M_{h} fitted as a free parameter in each stellar mass bin.

when the number of free parameters is taken into account, the EG model performs at least as well as the NFW fit. However, in order to really distinguish between these two models, we need to reduce the uncertainties in our measurement, in our lens modelling, and in the assumptions related to EG theory and halo model.

In order to further assess the quality of the EG prediction across the M_*-range, we determine the 'best' amplitude A_{B} and index n_{B}: the factors that minimize the χ^2 statistic when we fit:

$$\Delta\Sigma_{\mathrm{EG}}(A_{\mathrm{B}}, n_{\mathrm{B}}, R) = A_{\mathrm{B}} \frac{C_{\mathrm{D}}\sqrt{M_{\mathrm{b}}}}{4} \left(\frac{R}{h_{70}^{-1}\mathrm{kpc}} \right)^{-n_{\mathrm{B}}}, \qquad (33)$$

We find that the slope of the EG prediction is very close to the observed slope of the ESD profiles, with a mean value of $\langle n_{\mathrm{B}} \rangle = 1.01^{+0.02}_{-0.03}$. In order to obtain better constraints on A_{B}, we set $n_{\mathrm{B}} = 1$. The values of A_{B} (with 1σ errors) for the point mass are shown in Table 2. We find the amplitude of the point mass prediction to be consistently lower than the measurement. This is expected since the point mass approximation only takes the mass contribution of the central

galaxy into account, and not that of extended components like hot gas and satellites (described in Sect. 2.2). However, the ESD of the extended profile (which is shown in Fig. 3 for comparison) does not completely solve this problem. When we determine the best amplitude for the extended mass distribution by scaling its predicted ESD, we find that the values of $A_{\mathrm{B}}^{\mathrm{ext}}$ are still larger than 1, but less so than for the point mass (at a level of $\sim 1\sigma$, see Table 2). Nevertheless, the comparison of the extended ESD with the measured lensing profile yields a slightly higher reduced χ^2: $45.50/40 = 1.138$. However, accurately predicting the baryonic and apparent DM contribution of the extended density distribution is challenging (see Sect. 4.3). Therefore, the extended ESD profile can primarily be used as an indication of the uncertainty in the lens model.

6 CONCLUSION

Using the $\sim 180\,\mathrm{deg}^2$ overlap of the KiDS and GAMA surveys, we present the first test of the theory of emergent

gravity proposed in Verlinde (2016) using weak gravitational lensing. In this theory, there exists an additional component to the gravitational potential of a baryonic mass, which can be described as an *apparent* DM distribution. Because the prediction of the apparent DM profile as a function of baryonic mass is currently only valid for static, spherically symmetric and isolated mass distributions, we select $33,613$ central galaxies that dominate their surrounding mass distribution, and have no other centrals within the maximum radius of our measurement ($R_{\mathrm{max}} = 3\,h_{70}^{-1}\mathrm{Mpc}$). We model the baryonic matter distribution of our galaxies using two different assumptions for their mass distribution: the point mass approximation and the extended mass profile. In the point mass approximation we assume that the bulk of the galaxy's mass resides within the minimum radius of our measurement ($R_{\mathrm{min}} = 30\,h_{70}^{-1}\mathrm{kpc}$), and model the lens as a point source with the mass of the stars and cold gas of the galaxy. For the extended distribution, we not only model the stars and cold gas component as a Sérsic profile, but also try to make reasonable estimates of the extended hot gas and satellite distributions. We compute the lensing profiles of both models and find that, given the current statistical uncertainties in our lensing measurements, both models give an adequate description of isolated centrals. In this regime (where the mass distribution can be approximated by point mass) the lensing profile of apparent DM in EG is the same as that of the excess gravity in MOND[8], for the specific value $a_0 = cH_0/6$.

When computing the observed and predicted ESD profiles, we need to make several assumptions concerning the EG theory. The first is that, because EG gives an effective description of GR in empty space, the effect of the gravitational potential on light rays remains unchanged. This allows us to use the regular gravitational lensing formalism to measure the ESD profiles of apparent DM in EG. Our second assumption involves the used background cosmology. Because EG is only developed for present-day de Sitter space, we need to assume that the evolution of cosmological distances is approximately equal to that in ΛCDM, with the cosmological parameters as measured by Planck XIII (2015). For the relatively low redshifts used in this work ($0.2 < z_{\mathrm{s}} < 0.9$), this is a reasonable assumption. The third assumption is the value of H_0 that we use to calculate the apparent DM profile from the baryonic mass distribution. In an evolving universe, the Hubble parameter $H(z)$ is expected to change as a function of the redshift z. This evolution is not yet implemented in EG. Instead it uses the approximation that we live in a dark energy dominated universe, where $H(z)$ resembles a constant. We follow Verlinde (2016) by assuming a constant value, in our case: $H_0 = 70\,\mathrm{km\,s^{-1}Mpc^{-1}}$, which is reasonable at a mean lens redshift of $\langle z_{\mathrm{l}} \rangle \sim 0.2$. However, in order to obtain a more accurate prediction for the cosmology and the lensing signal in the EG framework, all these issues need to be resolved in the future.

Using the mentioned assumptions, we measure the ESD profiles of isolated centrals in four different stellar mass bins,

and compare these with the ESD profiles predicted by EG. They exhibit a remarkable agreement, especially considering that the predictions contain *no free parameters*: both the slope and the amplitudes within the four M_*-bins are completely fixed by the EG theory and the measured baryonic masses M_{g} of the galaxies. In order to perform a very simple comparison with ΛCDM, we fit the ESD profile of a simple NFW distribution (combined with a baryonic point mass) to the measured lensing profiles. This NFW model contains one free parameter, the halo mass M_{h}, for each stellar mass bin. We compare the reduced χ^2 of the NFW fit (which has 4 free parameters in total) with that of the prediction from EG (which has no free parameters). Although the NFW fit has fewer degrees of freedom (which slightly penalizes χ^2_{red}) the reduced χ^2 of this model is slightly lower than that of EG, where $\chi^2_{\mathrm{red,NFW}} = 0.933$ and $\chi^2_{\mathrm{red,EG}} = 1.121$ in the point mass approximation. For both theories, the value of the reduced χ^2 is well within reasonable limits, especially considering the very simple implementation of both models. The fact that our observed density profiles resemble both NFW profiles and the prediction from EG, suggests that this theory predicts a phenomenology very similar to a virialized DM halo. Using the Bayesian Information Criterion, we find that $BIC_{\mathrm{EG}} = 44.82$ and $BIC_{\mathrm{NFW}} = 48.33$. These BIC values imply that, taking the number of data points and free parameters into account, the EG prediction describes our data at least as well as the NFW fit. However, a thorough and fair comparison between ΛCDM and EG would require a more sophisticated implementation of both theories, and a full Bayesian analysis which properly takes the free parameters and priors of the NFW model into account. Nonetheless, given that the model uncertainties are also addressed, future data should be able to distinguish between the two theories.

We propose that this analysis should not only be carried out for this specific case, but on multiple scales and using a variety of different probes. From comparing the predictions of EG to observations of isolated centrals, we need to expand our studies to the scales of larger galaxy groups, clusters, and eventually to cosmological scales: the cosmic web, BAO's and the CMB power spectrum. Furthermore, there are various challenges for EG, especially concerning observations of dynamical systems such as the Bullet Cluster (Randall et al. 2008) where the dominant mass component appears to be separate from the dominant baryonic component. There is also ongoing research to assess whether there exists an increasing mass-to-light ratio for galaxies of later type (Martinsson et al. 2013), which might challenge EG if confirmed. We conclude that, although this first result is quite remarkable, it is only a first step. There is still a long way to go, for both the theoretical groundwork and observational tests, before EG can be considered a fully developed and solidly tested theory. In this first GGL study, however, EG appears to be a good parameter-free description of our observations.

---

[8] After this paper was accepted for publication, it was pointed out to us that Milgrom (2013) showed that galaxy-galaxy lensing measurements from the Canada-France-Hawaii Telescope Legacy Survey (performed by Brimioulle et al. 2013) are consistent with predictions from relativistic extensions of MOND up to a radius of $140\,h_{72}^{-1}\mathrm{kpc}$ (note added in proof).

Author contributions: All authors contributed to the development and writing of this paper. The authorship list is given in three groups: the lead authors (M. Brouwer & M. Visser), followed by two alphabetical groups. The first alphabetical group includes those who are key contributors to both the scientific analysis and the data products. The second group covers those who have either made a significant contribution to the data products, or to the scientific analysis.

REFERENCES

Abazajian K. N., et al., 2009, ApJS, 182, 543
Akaike H., 1973, Biometrika, 60, 255
Andrae R., Schulze-Hartung T., Melchior P., 2010, preprint, (arXiv:1012.3754)

Bartelmann M., Schneider P., 2001, Physics Reports, 340, 291
Bertin E., Arnouts S., 1996, A&AS, 117, 393
Betoule M., et al., 2014, A&A, 568, A22
Blake C., et al., 2011, MNRAS, 415, 2892
Boselli A., et al., 2010, PASP, 122, 261
Boselli A., Cortese L., Boquien M., Boissier S., Catinella B., Lagos C., Saintonge A., 2014, A&A, 564, A66
Bosma A., 1981, AJ, 86, 1791
Bower R. G., Benson A. J., Malbon R., Helly J. C., Frenk C. S., Baugh C. M., Cole S., Lacey C. G., 2006, MNRAS, 370, 645
Brimioulle F., Seitz S., Lerchster M., Bender R., Snigula J., 2013, MNRAS, 432, 1046
Brouwer M. M., et al., 2016, preprint, (arXiv:1604.07233)
Bruzual G., Charlot S., 2003, MNRAS, 344, 1000
Capaccioli M., Schipani P., 2011, The Messenger, 146, 2
Catinella B., et al., 2013, MNRAS, 436, 34
Cavaliere A., Fusco-Femiano R., 1976, A&A, 49, 137
Crocker A. F., Bureau M., Young L. M., Combes F., 2011, MNRAS, 410, 1197
Davis T. A., et al., 2013, MNRAS, 429, 534
Driver S. P., et al., 2011, MNRAS, 413, 971
Duffy A. R., Schaye J., Kay S. T., Dalla Vecchia C., 2008, MNRAS: Letters, 390, L64
Edge A., Sutherland W., Kuijken K., Driver S., McMahon R., Eales S., Emerson J. P., 2013, The Messenger, 154, 32
Eisenstein D. J., et al., 2005, ApJ, 633, 560
Erben T., et al., 2013, MNRAS, 433, 2545
Faulkner T., Guica M., Hartman T., Myers R. C., Van Raamsdonk M., 2014, Journal of High Energy Physics, 3, 51
Fedeli C., Semboloni E., Velliscig M., Van Daalen M., Schaye J., Hoekstra H., 2014, J. Cosmology Astropart. Phys., 8, 028
Fenech Conti I., et al., 2016, (in prep.)
Fischer P., et al., 2000, AJ, 120, 1198
Foreman-Mackey D., Hogg D. W., Lang D., Goodman J., 2013, PASP, 125, 306
Hildebrandt H., et al., 2016, preprint, (arXiv:1606.05338)
Hoekstra H., Yee H. K. C., Gladders M. D., 2004, ApJ, 606, 67
Hoekstra H., Herbonnet R., Muzzin A., Babul A., Mahdavi A., Viola M., Cacciato M., 2015, MNRAS, 449, 685
Hunter J. D., et al., 2007, Computing in science and engineering, 9, 90
Jacobson T., 1995, Physical Review Letters, 75, 1260
Jacobson T., 2016, Physical Review Letters, 116, 201101
de Jong J. T. A., Kleijn G. A. V., Kuijken K. H., Valentijn E. A., et al., 2013, Experimental Astronomy, 35, 25
Kahn F. D., Woltjer L., 1959, ApJ, 130, 705
Kass R. E., Raftery A. E., 1995, Journal of the American Statistical Association, 90, 773
Kelvin L. S., et al., 2012, MNRAS, 421, 1007
Kessler R., et al., 2009, ApJS, 185, 32
Kuijken K., et al., 2011, The Messenger, 146
Kuijken K., et al., 2015, MNRAS, 454, 3500
Liddle A. R., 2007, MNRAS, 377, L74
von der Linden A., et al., 2014, MNRAS, 439, 2
Liske J., et al., 2015, MNRAS, 452, 2087
Mandelbaum R., 2015, in Cappellari M., Courteau S., eds, IAU Symposium Vol. 311, Galaxy Masses as Constraints of Formation Models. pp 86–95 (arXiv:1410.0734)
Mandelbaum R., Seljak U., Kauffmann G., Hirata C. M., Brinkmann J., 2006, MNRAS, 368, 715
Martinsson T. P. K., Verheijen M. A. W., Westfall K. B., Bershady M. A., Andersen D. R., Swaters R. A., 2013, A&A, 557, A131
McCarthy I. G., et al., 2010, MNRAS, 406, 822
McGaugh S. S., Lelli F., Schombert J. M., 2016, Physical Review Letters, 117, 201101
Mentuch Cooper E., et al., 2012, ApJ, 755, 165
Milgrom M., 1983, ApJ, 270, 371

Milgrom M., 2013, Physical Review Letters, 111, 041105

Miller L., Kitching T., Heymans C., Heavens A., van Waerbeke L., 2007, MNRAS, 382, 315

Miller L., et al., 2013, MNRAS, 429, 2858

Morokuma-Matsui K., Baba J., 2015, MNRAS, 454, 3792

Mulchaey J. S., 2000, ARA&A, 38, 289

Mulchaey J. S., Davis D. S., Mushotzky R. F., Burstein D., 1996, ApJ, 456, 80

Navarro J. F., Frenk C. S., White S. D., 1995, MNRAS, 275, 56

Padmanabhan T., 2010, Reports on Progress in Physics, 73, 046901

Peebles P. J., Yu J., 1970, ApJ, 162, 815

Pérez F., Granger B. E., 2007, Computing in Science & Engineering, 9, 21

Planck XIII x., 2015, preprint, (arXiv:1502.01589)

Pohlen M., et al., 2010, A&A, 518, L72

Randall S. W., Markevitch M., Clowe D., Gonzalez A. H., Bradač M., 2008, ApJ, 679, 1173

Riess A. G., Press W. H., Kirshner R. P., 1996, ApJ, 473, 88

Rines K., Geller M. J., Diaferio A., Kurtz M. J., 2013, ApJ, 767, 15

Robotham A. S., et al., 2011, MNRAS, 416, 2640

Rubin V. C., 1983, Scientific American, 248, 96

Saintonge A., et al., 2011, MNRAS, 415, 32

Schaye J., et al., 2010, MNRAS, 402, 1536

Schneider P., Kochanek C., Wambsganss J., 2006, Gravitational Lensing: Strong, Weak and Micro: Saas-Fee Advanced Course 33.   Vol. 33, Springer Science & Business Media

Schwarz G., 1978, Annals of Statistics, 6, 461

Sérsic J. L., 1963, Boletin de la Asociacion Argentina de Astronomia La Plata Argentina, 6, 41

Sersic J. L., 1968, Atlas de galaxias australes

Sifón C., et al., 2015, MNRAS, 454, 3938

Spergel D. N., et al., 2003, ApJS, 148, 175

Springel V., et al., 2005, Nature, 435, 629

Sun M., Voit G. M., Donahue M., Jones C., Forman W., Vikhlinin A., 2009, ApJ, 693, 1142

Taylor E. N., et al., 2011, MNRAS, 418, 1587

van Uitert E., et al., 2016, MNRAS,

Velander M., et al., 2014, MNRAS, 437, 2111

Verlinde E., 2011, Journal of High Energy Physics, 4, 29

Verlinde E. P., 2016, preprint, (arXiv:1611.02269)

Viola M., et al., 2015, MNRAS, 452, 3529

White S. D., Rees M., 1978, MNRAS, 183, 341

Wright C. O., Brainerd T. G., 2000, ApJ, 534, 34

Zwicky F., 1937, ApJ, 86, 217

de Jong J. T. A., et al., 2015, A&A, 582, A62

This paper has been typeset from a TeX/LaTeX file prepared by the author.